3-30-2010

Guest-free monolayer clathrate and its coexistence with two-dimensional high-density ice

Jaeil Bai
University of Nebraska-Lincoln, jbai2@unl.edu

C. Austen Angell
Arizona State University

Xiao Cheng Zeng
University of Nebraska-Lincoln, xzeng1@unl.edu

Guest-free monolayer clathrate and its coexistence with two-dimensional high-density ice

Jaeil Bai[a], C. Austen Angell[b], and Xiao Cheng Zeng[a,1]

[a]Department of Chemistry and Nebraska Center for Materials and Nanoscience, University of Nebraska, Lincoln, NE, 68588; and [b]Department of Chemistry, Arizona State University, Tempe, AZ, 85287

Edited* by H. Eugene Stanley, Boston University, Boston, MA, and approved February 23, 2010 (received for review June 10, 2009)

Three-dimensional (3D) gas clathrates are ice-like but distinguished from bulk ices by containing polyhedral nano-cages to accommodate small gas molecules. Without space filling by gas molecules, standalone 3D clathrates have not been observed to form in the laboratory, and they appear to be unstable except at negative pressure. Thus far, experimental evidence for guest-free clathrates has only been found in germanium and silicon, although guest-free hydrate clathrates have been found, in recent simulations, able to grow from cold stretched water, if first nucleated. Herein, we report simulation evidence of spontaneous formation of monolayer clathrate ice, with or without gas molecules, within hydrophobic nano-slit at low temperatures. The guest-free monolayer clathrate ice is a low-density ice (LDI) whose geometric pattern is identical to Archimedean $4 \cdot 8^2$-truncated square tiling, i.e. a mosaic of tetragons and octagons. At large positive pressure, a second phase of 2D monolayer ice, i.e. the puckered square high-density ice (HDI) can form. The triple point of the LDI/liquid/HDI three-phase coexistence resembles that of the ice-I_h/water/ice-III three-phase coexistence. More interestingly, when the LDI is under a strong compression at 200 K, it transforms into the HDI via a liquid intermediate state, the first direct evidence of Ostwald's rule of stages at 2D. The tensile limit of the 2D LDI and water are close to that of bulk ice-I_h and laboratory water.

2D high-density ice | 2D low-density ice | 2D monolayer ice clathrate | Ostwald rule of stages | tensile limit of 2D liquid

Natural gas is largely reserved in nature in the form of gas clathrates on the world's ocean floors (1–7). In the laboratory, gas clathrates can be produced by bringing a nonpolar gas in direct contact with liquid water under moderate pressure and at low temperature (1, 8–11). Since gas clathrates possess an open-cage structure to accommodate small gas molecules, gas clathrates can be characterized by two parameters: (1) the minimum gas pressure needed to stabilize the clathrates, and (2) the degree of occupancy or the fraction of cages occupied by the gas molecules. Although structural and thermodynamic properties of many gas clathrates are well characterized, the kinetic process of 3D clathrate formation is still less understood (1, 12). In an attempt to gain molecular insight into kinetics of clathrate formation, we carried out molecular dynamics (MD) simulations of clathrate formation within a slit nanopore whose width D is on the scale of 0.6 nm (see *Materials and Methods*). Because the slit nanopore can only accommodate one molecular layer of water, the timescale required for the formation of the quasi-2D gas clathrate is within the reach of MD simulation (typically $10–10^2$ ns).

Results and Discussions

We first considered a binary fluid mixture of water and argon (with 11.1% mole fraction of Ar) confined to the slit nanopore ($D = 0.62$ nm) whose two opposing walls are smooth and hydrophobic (13–15). The fluid mixture was initially equilibrated at a constant temperature ($T = 1000$ K) and a constant lateral pressure ($p_{xy} = 500$ MPa) and then subjected to an instantaneous quench to $T = 250$ K. After 30 ns equilibration, a monolayer gas clathrate was observed, as shown in Fig. 1*A* (and Movie S1). Interestingly, the hydrogen-bonding network of the gas clasthrate exhibits a geometry known as *Archimedean* $4 \cdot 8^2$ truncated square tiling, i.e. a mosaic of tetragons and octagons.

At maximum (100%) occupancy, when each octagon contains an argon atom, the mole fraction of Ar would be 20%. In practice it is difficult to achieve full occupancy in MD simulations due to the strong hydrophobic attraction among argon atoms. As an example, we considered a water-argon fluid mixture (with ~19.7% mole fraction of Ar) confined to the same slit nanopore. The mixture was first equilibrated at a constant lateral pressure of 1 GPa and $T = 1,000$ K, and then quenched to 250 K and held for 150 ns. Argon occupancy of only ~65% was attained. When the simulation was extended for additional 70 ns (with temperature and pressure set to $T = 270$ K and $p_{xy} = 1.5$ GPa), a much higher argon occupancy, ~78%, was achieved (Fig. 1*B*). Still, a small domain of phase-separated argon fluid remained within the monolayer gas clathrate.

While guest molecules are necessary for stabilization of the open lattice structure of 3D gas clathrates of water at ambient pressure, it is known that a guest-free clathrate of germanium can be synthesized (16), and an almost empty clathrate of Si has been described (17, 18). The latter can definitely be formed in simulations with the Stillinger-Weber potential (19). It is clearly a question of interest whether a guest-free clathrate of water is achievable under *any* circumstances. We note that Wang and coworkers (20) reported a monolayer ice structure of chemisorbed water on a surface of hydroxylated silica at 0 K (20). This chemsorption-based ice structure resembles the *Archimedean* $4 \cdot 8^2$ truncated square tiling but it is not freestanding because of strong interaction between water and the underlying substrate. Molinero and coworkers (11) showed that, in their 3D *mW* model, empty clathrates could form but only at large negative pressures. Fennell and Gezelter reported a MD simulation of spontaneous formation of a guest-free ice-clathrate structure (ice-*i*) from a soft-sticky-dipole liquid (a model of water) at a low temperature (21). The projection of the *ice-i* onto a 2D plane along a particular direction gives rise to the *Archimedean* $4 \cdot 8^2$ truncated square tiling. Later, however, Fennell and Gezelter showed that the stability of *ice-i* can be model-dependent (22), and the spontaneous formation of ice-*i*-like structure based on more realistic models of water (such as TIP5P) is yet to be seen. Here we study the question of spontaneous formation for the network structure of *Archimedean* $4 \cdot 8^2$ truncated square tiling.

We first performed a MD simulation of pure water confined to the slit nanopore ($D = 0.557$ nm) using the constant lateral pressure and constant temperature ($Np_{xy}T$) ensemble. The confined

Author contributions: J.B., A.A., and X.C.Z. designed research; J.B., A.A., and X.C.Z. performed research; J.B. and X.C.Z. contributed new reagents/analytic tools; J.B., A.A., and X.C.Z. analyzed data; and J.B., A.A., and X.C.Z. wrote the paper.

The authors declare no conflict of interest.

*This Direct Submission article had a prearranged editor.

[1]To whom correspondence should be addressed. E-mail: xczeng@phase2.unl.edu.

This article contains supporting information online at www.pnas.org/cgi/content/full/0906437107/DCSupplemental.

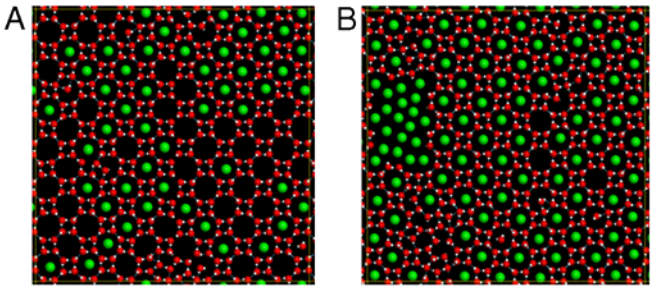

Fig. 1. (*A*) A snapshot of quenched molecular coordinates of the monolayer gas clathrate formed in between two hydrophobic walls ($D = 0.62$ nm) at 250 K and under 500 MPa lateral pressure. Mole fraction of argon is 11.1%. (*B*) A snapshot of quenched molecular coordinates of the monolayer gas clathrate formed in between two hydrophobic walls ($D = 0.62$ nm) at 270 K and under 1.5 GPa lateral pressure. Mole fraction of argon is 19.7%. Argon occupancy in water octagons is ~78%. Red spheres represent oxygen, white spheres hydrogen, green spheres argon, and blue dotted lines hydrogen bonds.

liquid water was initially equilibrated at $T = 320$ K and $p_{xy} = 1$ MPa. The temperature of the system was then lowered in six steps to $T = 260$ K. At each temperature step, a simulation time of 20 ns was used. Based on the equilibrated system at 260 K, six independent MD simulations were carried out next, all subjected to an instantaneous quench to $T = 250$ K with the lateral pressure controlled at $p_{xy} = 500, 100, 50, 5, -5$, and -50 MPa, respectively. *Spontaneous* formation of 2D crystalline structures (Movie S2) was observed in five simulations except for $p_{xy} = 500$ MPa (for which the liquid was in a supercooled state). Remarkably, the 2D crystalline structures (other than some polygonal defects) are identical to the water network structure of the monolayer gas clathrate, i.e. a mosaic of tetragons and octagons. A snapshot of the final configuration of the 2D crystalline structure for $p_{xy} = -50$ MPa is shown in Fig. 2*A*, where the area density N/A (water molecules per unit area) is ~8.94/nm^2. Note that the water network of the monolayer gas clathrate satisfies the ice rule (i.e., every water molecule is hydrogen-bonded to exactly four nearest-neighbor water molecules) due to the three-centered hydrogen-bonding interaction between any two neighbor tetragons (Fig. 2*B*).We therefore name the water network of the monolayer gas clathrate a 2D low-density ice (LDI).

Simulations using larger slit widths in the range of $D =$ 0.50–0.68 nm show that more negative lateral pressures are needed to stabilize the LDI phase as the slit width increases. For instance, with $D = 0.575$ nm, spontaneous formation of 2D LDI is not observed at *any* positive pressure, in contrast to the slit $D = 0.557$ nm case described above; at $T = 250$ K, LDI only forms at $p_{xy} = -5$ MPa. However, if polygonal defects are present, the defects will promote void nucleation and eventually can lead to structural raptures (23, 24). For example, a snapshot of void-containing LDI is shown in Fig. 2*C*. Clearly, polygonal defects tend to accumulate near the edge of the 2D void. Once formed, the void grows larger, and faster, and eventually the LDI will be ruptured.

On the other hand, when the confined water is at a high positive pressure, a form of 2D high-density ice (HDI), i.e. the puckered monolayer square ice (Fig. 2*D*) can form spontaneously (25, 26). Note that Zangi and Mark (25) observed the spontaneous crystallization of the puckered monolayer square ice within two *atomically rough* walls of model quartz, while Koga and Tanaka (26) observed the same ice structure within two *atomically smooth* walls, which indicate that the formation of 2D HDI ice is insensitive to detailed atomic structure of the walls but only to the hydrophobic confinement. To confirm that the formation of the LDI is insensitive to the atomic structure of the wall surface, we performed an independent constant-volume and constant-temperature (NVT) MD simulation for water confined to two single graphene layers (see *Materials and Methods*). Again, spontaneous formation of LDI at 210 K is observed in less than 2 ns. A snapshot of the LDI configuration at 8 ns is displayed in Fig. S1.

It is known that bulk ice has 15 crystalline polymorphs [named using Roman numerals (27)] and most of them are stable only at high pressures. However, the number of 2D polymorphs for monolayer ice is much smaller than 15 because of the restrictions involved in satisfying the ice rule in 2D while simultaneously tiling the plane seamlessly. Can the 2D LDI undergo a phase transition to 2D HDI at high lateral pressure? To address this question, we explored p_{xy}-T phase diagram of the monolayer water confined to a slit nanopore ($D = 0.65$ nm) through five independent MD simulations using the $NP_{xy}T$ ensemble, where $T = 200$, 220, 230, 240, and 250 K, respectively. In all five simulations, the initial pressure was set to $p_{xy} = -100$ MPa and the initial configurations were chosen to be a perfect LDI (Fig. 2*A*), with the following results:

1. For $T = 250$ K, the LDI melts into a liquid due to the larger width ($D > 0.6$ nm). As p_{xy} is increased from -100 to 600 MPa in steps (20 ns per step), a phase transition from the liquid to the puckered square HDI occurs at $p_{xy} \sim 400$ MPa, as shown in Fig. 3*A*. By contrast, when p_{xy} is decreased in steps (20 ns per step) from 600 to -100 MPa with a perfect HDI as the initial structure, no HDI-to-liquid transition was observed since the area density of the HDI shows little change (Fig. 3*A*), indicating a high free-energy barrier that separates the HDI and liquid state at 250 K. However, if some defects are deliberately introduced into the HDI to speed up nucleation process, a HDI-to-liquid transition was observed at 50 MPa within a few ns. The high free-energy barrier and large hysteresis loop suggests that the liquid-to-HDI transition is a strong first-order phase transition even though the transition is quasi-2D in nature (28).
2. For $T = 240$ K, the LDI is stable at the lowest pressure $p_{xy} = -100$ MPa. As p_{xy} is increased from -100 to 600 MPa

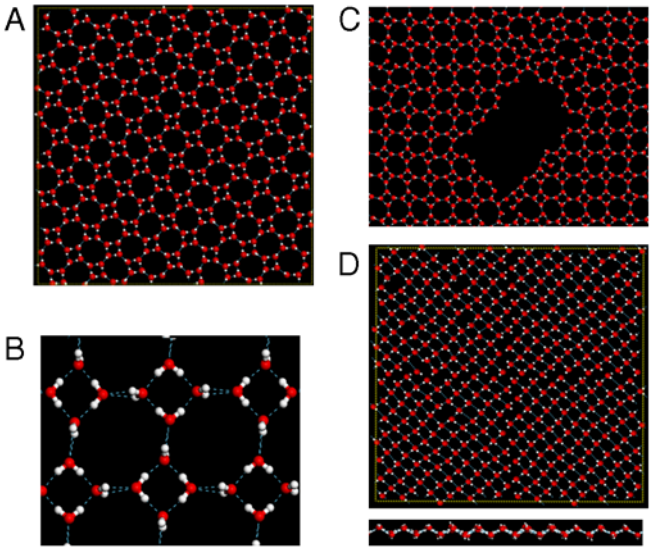

Fig. 2. (*A*) A snapshot of quenched molecular coordinates of 2D monolayer low-density ice (LDI) formed in between two hydrophobic walls ($D =$ 0.557 nm). The geometric pattern of the LDI is identical to *Archimedean* $4 \cdot 8^2$ truncated square tiling, composed of water tetragons and octagons. (*B*) A zoomed view of intermolecular hydrogen bonds (blue dotted lines). Three-centered hydrogen bonds can be seen in horizontal direction. (*C*) A cavity (void) is nucleated inside the LDI. The system is in between two hydrophobic walls ($D = 0.59$ nm, $T = 240$ k). (*D*) Top view (top) and side view (bottom) of a snapshot of quenched molecular coordinates of 2D monolayer high-density ice (HDI) formed in between two hydrophobic walls ($D = 0.65$ nm).

in steps (20 ns per step), two phase transitions occur, one from the LDI to liquid at $p_{xy} \sim 50$ MPa and another from liquid to HDI at $p_{xy} \sim 280$ MPa, as shown in Fig. 3*A*. This 2D solid-to-liquid-to-solid phase transition is similar to the bulk ice I_h-to-liquid water-to-ice III phase transition (27).

3. For $T = 230$ K, a similar solid-to-liquid-to-solid phase transition occurs, one at $p_{xy} \sim 100$ MPa while another at $p_{xy} \sim 180$ MPa. The fact that the LDI-to-liquid transition occurs at higher p_{xy} and lower T indicates that the liquidus line of the 2D LDI has a negative slope like that of bulk ice I_h. Clearly, from the Clapeyron equation, the density of 2D LDI is lower than that of 2D liquid.
4. For $T = 220$ K, the solid-to-liquid-to-solid transition disappears. Rather, a strong first-order LDI-to-HDI transition can be seen at $p_{xy} \sim 250$ MPa as p_{xy} is increased from −100 to 600 MPa in steps (Fig. 3*A*). This solid-to-solid phase transition resembles the ice I_h-to-ice III transition in bulk.
5. For $T = 200$ K, again, a strong first-order LDI-to-HDI transition occurs, but at a pressure $p_{xy} \sim 400$ MPa (Fig. 3*A*).

Figure 3*B* displays an approximate p_{xy}-T phase diagram, based on results of the latter five MD simulations (the true phase boundary can be determined via the two-phase coexistence method, e.g. ref. 29). A triple point for LDI-liquid-HDI three-phase coexistence is possibly located between 220–230 K and 100–180 MPa. The triple point resembles the bulk ice I_h-liquid-ice III triple point (27). As in the 3D system, the LDI-HDI phase boundary exhibits a positive slope while the LDI-liquid phase boundary exhibits a negative slope.

As might be expected from the behavior of the bulk phases, both liquid and crystal phases of 2D water exhibit tensile limits. The tensile limit represents the release of a metastable state and hence has a time dependence related to nucleation probabilities. In 3D systems the nucleation probability is an extremely sharp function of T, P near the homogeneous nucleation limit but the problem has been little explored in reduced dimensionality. In our computer experiments, these are sharply defined and reproducible at a fixed rate of increase of the lateral tension which we applied stepwise by increasing the tension 100 or 20 MPa each 300 ps, at each temperature (see *Materials and Methods*)

The results are combined with the melting and crystal/crystal phase transitions to give the approximate phase diagram of 2D ice presented in Fig. 3*B*, including tensile limits of the 2D system. Its form may be compared with the phase diagrams presented elsewhere for 3D (TIP4P) ice (24) and laboratory water (23). Although it may be no more than the difference between two alternative potentials, the present TIP5P 2D ice (at $D = 0.65$ nm) appears to have *a higher tensile limit than 3D ice* (1.4 ± 0.1 GPa vs. 1.0 GPa), while the tensile limit of the 2D liquid at 270 K, 115 ± 9 MPa is lower than the measured tensile limit of 3D liquid water (140 MPa) (23). We are surprised by the overall degree of similarity, which may be coincidental. Note that a spinodal limit at 298 K determined recently for two-layer water confined between structured hydrophobic walls (30), of comparable separation, was nearly twice as negative as the tensile limit estimated here. As always, the distinction between behavior of perfect crystal, and surface-free, systems of simulation, and the behavior of real systems with defects and interfaces, must be taken into account when assessing the results of these calculations. The difference between true equilibrium and spinodal limits to phase stability [two-phase versus one-phase melting, for instance (24)] will be evaluated in future work.

Besides metastability of water under tension (i.e. at negative pressure), there is also much interest in the metastability of water in the supercooled state. Bulk water, when supercooled, can exhibit unique phase behavior such as (controversially) a liquid-to-liquid transition from low-density liquid (LDL) to high-density liquid (HDL) (31–39). Can the 2D monolayer water, when supercooled, also undergo a liquid-to-liquid phase transition? To explore this possibility, we performed an additional three independent MD simulations using a quenching technique. Initially, a sample of water confined to a slit nanopore ($D = 0.65$ nm) was equilibrated at $T = 250$ K and $p_{xy} = -80$, -20, and 60 MPa, respectively. Each system was then quenched instantaneously to 200 K, followed by 20 ns MD simulation in the $NP_{xy}T$ ensemble.

Interestingly, for two systems at $p_{xy} = -80$ and -20 MPa, we found that the liquid freezes spontaneously into the LDI phase with a small domain of HDI trapped in the middle of LDI during the crystal growth. The overall area density of the LDI/HDI structure is 9.87 (Fig. 4*A*) and 9.91 nm^{-2}, respectively. Conversely, for the system at $p_{xy} = 60$ MPa, the liquid freezes spontaneously into

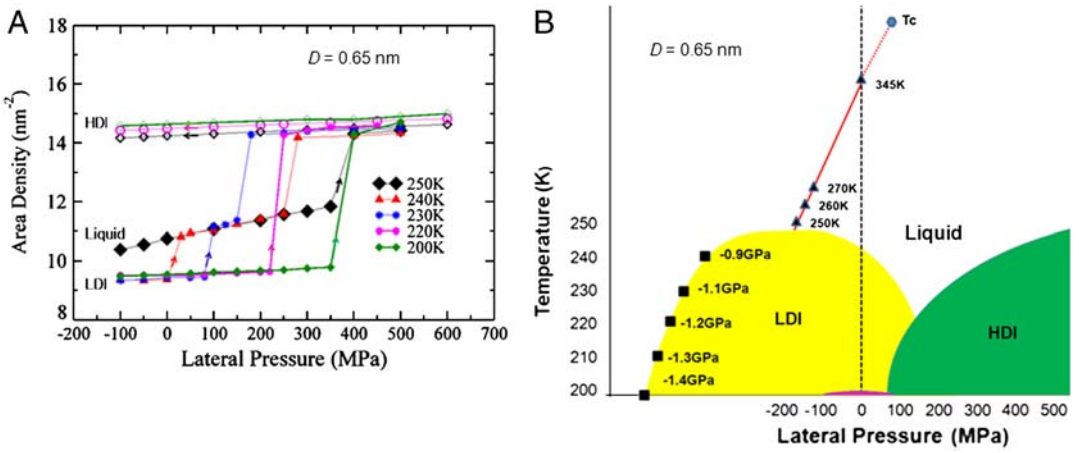

Fig. 3. (*A*) Isotherms (200–250 K) of water confined to two hydrophobic walls ($D = 0.65$ nm). The lateral pressure is increased stepwise from −100 to 600 MPa (solid symbols), and then decreased from 600 to −100 MPa in steps (open symbols). The system is initially in the liquid state (250 K) or in the solid LDI state (200–240 K). (*B*) An approximate p_{xy}-T phase diagram for the $D = 0.65$ nm case of monolayer water confined between the two hydrophobic walls. A triple point for LDI-liquid-HDI three-phase coexistence is estimated to be located between 220–230 K and 100–180 MPa. The triple point bears resemblance to the bulk ice I_h-liquid-ice III triple point. The small pink area at the bottom of the figure represents the *P-T* domain in which HDI and LDI form sequentially from supercooled water, and then coexit at 200 K. For narrower slits ($D < 0.65$ nm) the triple point is expected to move to higher pressures. Estimated tensile limits of the perfect LDI at temperature 200–240 K (black squares) and 2D liquid at temperature 250–270 K and 350 K (black triangles) are shown in a region of negative pressures. The red solid line shows the tensile limit of the liquid from 250 K to the critical temperature T_c of the 2D liquid, but the positive pressure component (red dashed line) is only schematic. The vertical black dashed line denotes zero pressure.

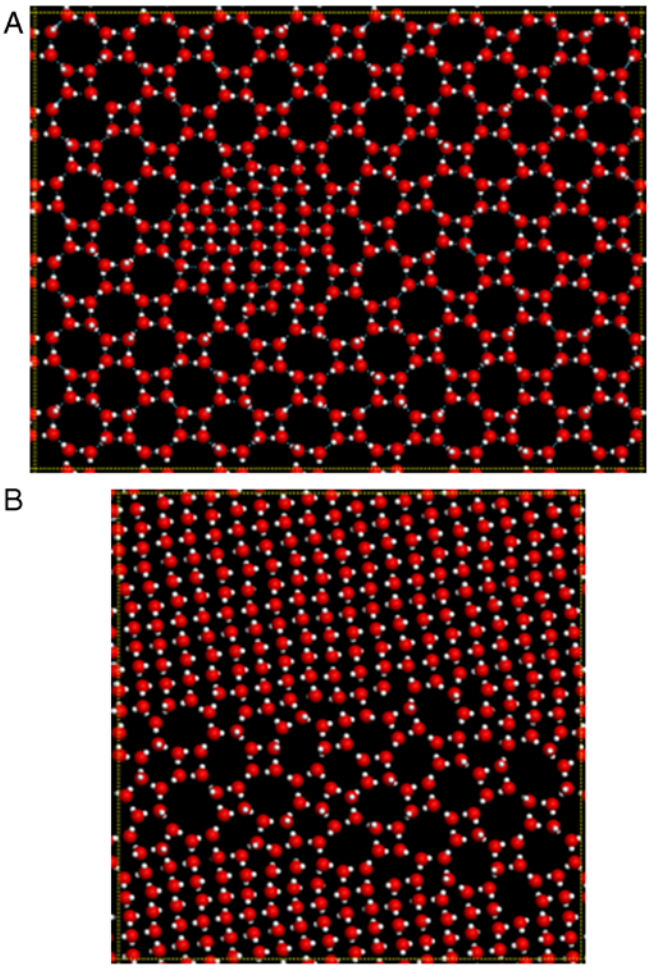

Fig. 4. A snapshot of quenched molecular coordinate of the coexisting LDI/HDI structure, formed spontaneously in between two hydrophobic walls ($D = 0.65$ nm) when the water is supercooled instantaneously from 250 to 200 K at (*A*) −80 MPa and (*B*) 60 MPa lateral pressure.

an HDI phase while a domain of LDI forms in the midst of crystal growth of HDI. The overall area density is 12.9 nm^{-2} (Fig. 4*B*). Hence, for 2D monolayer water, the fast kinetics of crystallization at temperatures around 200 K prevents the formation of LDL or HDL. In the pressure range of −80 to 60 MPa and below 210 K (see pink region in Fig. 3*B*), the sequential formation of two dramatically different phases of ice becomes a preferred mechanism for relieving the metastability of the supercooled state. Depending on which phase is nucleated first, the formation of the second phase (likely the metastable phase) will be promoted increasingly as the crystallization proceeds. In any case, when the coexisting LDI/HDI is subjected to a strong pressure $p_{xy} > 100$ MPa a direct solid-to-solid transition (from LDI-to-HDI) occurs within a few tens of nanoseconds at $T = 200$ K (Movie S3). On the other hand, when the coexisting LDI/HDI is subjected to a strong negative pressure $p_{xy} = -200$ MPa, a direct solid-to-solid transition (from HDI-to-LDI) was not observed within a few tens of nanoseconds at $T = 200$ K, indicating considerably slower transition kinetics compared to the LDI-to-HDI transition. When the temperature was raised to $T = 220$ K, evidence of direct HDI-to-LDI transition could be observed after 70 ns. Lastly, when the temperature was raised to $T = 230$ K, the HDI (containing a LDI grain) melted into liquid under the tension and then transformed into LDI (Movie S4).

The appearance of a liquid intermediate state in between the solid-to-solid transition is an interesting phenomenon, first recognized by Ostwald in 1897 (40). To our knowledge, this phenomenon has not been reported for crystallization in 2D materials. Can the same behavior be observed from 2D? To address this question, we examined dynamic trajectory of the simulation 5 described above, that is, the LDI is under a strong compression (400 MPa) at a low temperature (200 K). Remarkably, the dynamic trajectory shows that the LDI melted into a (short-lived) liquid before transforming into the HDI (Movie S5). At 200 K, the liquid is indeed the least stable state. Nevertheless, crystallization of the 2D HDI proceeds from the least stable state—2D liquid—is consistent with Ostwald's prediction ("rule of stages"). We note that a similar evidence of crystal growth through intermediate unstable states has been recently revealed in a 3D material (41).

Materials and Methods

Molecular Dynamics Simulation. Two types of walls for the slit nanopore were considered: (1) a rigid and smooth hydrophobic wall, and (2) a rigid single graphene layer. The wall-wall separation was set to accommodate just one layer of water (26). The TIP5P model was used for the water (42). For the smooth wall, we opted the 9-3 Lennard-Jones (LJ) potential for the water-hydrophobic wall interaction (13–15, 43). The MD simulations were performed using the constant lateral pressure and constant temperature ($Np_{xy}T$) ensemble. The periodic boundary conditions were applied in the lateral direction (x and y) in parallel with the two walls. The simulation supercell contains 400 water molecules, with or without argon atoms (the LJ parameters for argon are $\sigma_{Ar} = 3.40$ Å and $\varepsilon_{Ar} = 0.238$ kcal/mol). The cross LJ interaction parameters between Ar and TIP5P water were given by Lorentz-Berthelot rule. The Ar-wall interaction is described by the 9-3 LJ potential function, $U = \varepsilon\left(\frac{\sigma^9}{z^9} - \frac{\sigma^3}{z^3}\right)$, where the LJ parameters are $\sigma_{Ar\text{-}wl} = 2.430$ Å and $\varepsilon_{Ar\text{-}wl} = 2.965$ kcal/mol. The oxygen-wall interaction is also described by the 9-3 LJ potential with LJ parameters $\sigma_{O\text{-}wl} = 2.4737$ Å and $\varepsilon_{O\text{-}wl} = 1.2024$ kcal/mol. These parameters are almost the same as those used in a previous comprehensive study of the phase diagram of TIP5P water in the slit nanopore (44).

For the graphene wall, the C-C distance is fixed at 1.405 Å. The LJ parameters for carbon and oxygen interaction are $\sigma_{C\text{-}O} = 3.26$ Å and $\varepsilon_{C\text{-}O} = 0.1173$ kcal/mol (derived based on the Lorentz-Berthelot rule and the LJ parameters given in ref. 45 for TIP3P water model). The distance between the two graphene, namely, from the carbon center of one layer to the carbon center of the opposing layer, is fixed at 0.65 nm. The MD simulations were performed using constant volume and constant temperature (NVT) ensemble. The simulation supercell contains 400 water molecules. The area density of water is 9.02/nm^2.

All intermolecular interactions, including the long-range charge-charge interaction and the LJ interaction between oxygen atoms, were truncated at 8.75 Å by a switching function (26).

Structural Analysis. Instantaneous configurations (snapshots) generated in the MD simulations were mapped onto corresponding potential-energy local-minimum configurations using a steepest-descent method (at constant volume) (14).

Estimation of Tensile Limits. Tensile limits of 2D liquid and ice were estimated via a sequential series of MD simulations in the $Np_{xy}T$ ensemble. The initial pressure was set at $p_{xy} = -100$ MPa. Subsequently, the liquid (or ice) was subjected to an incremental of negative pressure of 20 (or 100) MPa per 300 ps, i.e., at an average tensile rate ~20 (or 100) MPa/300 ps. At the tensile limits, notable voids can be observed typically within a very short period of MD time (<100 ps).

Note Added in Proof.

During review of the manuscript, we learned a major breakthrough in simulating spontaneous 3D methane hydrate nucleation and growth (46).

ACKNOWLEDGMENTS. The authors are grateful to Professor Peter Rossky for valuable discussions. C.A.A. was supported by the National Science Foundation (DMR-0404714) and X.C.Z. was supported by the Department of Energy (DE-FG02-04ER46164), the Nebraska Research Initiative, and the University of Nebraska Holland Computer Center.

1. Sloan ED, Jr (2003) Fundamental principles and application of natural gas hydrates. *Nature* 426:353–359.
2. Hesselbo SP, et al. (2000) Massive dissociation of gas hydrate during a Jurassic oceanic anoxic event. *Nature* 406:392–395.
3. Makogon YF (1997) *Hydrates of Hydrocarbons* (Pennwell Books, Tulsa).
4. Kvenvolden KA (1998) *Methane Hydrate: Resources in the Near Future?* (Proc Int Symp Japan National Oil Company, Chiba City, Japan).
5. Fehn U, Snyder G, Edgberg PK (2000) Dating of pore wastes with ^{129}I: Relevance for the origin of marine gas hydrates. *Science* 289:2332–2335.
6. van der Waals JH, Platteeuw JC (1959) Clathrate solutions. *Adv Chem Phys* 2:1–57.
7. Barrer RM, Edge AVJ (1967) Gas hydrate containing argon, krypton and xenon. *Proc R Soc Lon Ser-A* 300:1–24.
8. Davidson DW (1973) *Water: A Comprehensive Treatise*, ed F Franks (Plenum, New York), Vol 2, pp 115–234.
9. Davidson DW, Handa YP, Ratcliffe CI, Tse JS, Powell BM (1984) The ability of small molecules to form clathrate hydrates of structure II. *Nature* 311:142–143.
10. Ripmeester JA, Ratcliffe CI, Powell BM (1987) A new clathrate hydrate structure. *Nature* 325:135–136.
11. Jacobson LC, Hujo W, Molinero V (2009) Thermodynamic stability and growth of guest-free clathrate hydrates: A low-density crystal phase of water. *J Phys Chem B* 113:10298–10307.
12. Tanaka H, Kiyohara K (1993) On the thermodynamic stability of clathrate hydrate. I.. *J Chem Phys* 98:4098–4109.
13. Lee SH, Rossky PJ (1994) A comparison of the structure and dynamics of liquid water at hydrophobic and hydrophilic surfaces—a molecular dynamics simulation study. *J Chem Phys* 100:3334–3345.
14. Koga K, Tanaka H, Zeng XC (2000) First-order transition in confined water between high-density liquid and low-density amorphous phases. *Nature* 408:564–567.
15. Yasuoka K, Gao GT, Zeng XC (2000) Molecular dynamics simulation of supersaturated vapor nucleation in slit pore. *J Chem Phys* 112:4279–4285.
16. Guloy AM, et al. (2006) A guest-free germanium clathrate. *Nature* 443:320–323.
17. Gryko J, et al. (2000) Low-density framework form of crystalline silicon with a wide optical band gap. *Phys Rev B* 62:R7707–R7710.
18. Ammar A, et al. (2004) On the clathrate form of elemental silicon, Si_{136}: Preparation and characterization of Na_xSi_{136} ($x \rightarrow 0$). *Solid State Sci* 6:393–400.
19. Wilson M, McMillan PF (2003) Crystal-liquid phase relations in silicon at negative pressure. *Phys Rev Lett* 90:135703-1–135703-4.
20. Yang J, Meng S, Xu LF, Wang EG (2004) Ice tessellation on a hydroxylated silica surface. *Phys Rev Lett* 92:146102-1–146102–4.
21. Fennell CJ, Gezelter JD (2004) On the structural and transport properties of the soft sticky dipole and related single-point water models. *J Chem Phys* 120:9175–9184.
22. Fennell CJ, Gezelter JD (2005) Computational free energy studies of a new ice polymorph which exhibits greater stability than ice I_h. *J Chem Theory Comput* 1:662–667.
23. Zheng Q, Durben DJ, Wolf GH, Angell CA (1991) Liquids at large negative pressures: Water at the homogeneous nucleation limit. *Science* 254:829–832.
24. Sciortino F, et al. (1995) Crystal stability limits at positive and negative pressures and the crystal-to-amorphous transition. *Phys Rev E* 52:6484–6491.
25. Zangi R, Mark AE (2003) Monolayer ice. *Phys Rev Lett* 91:025502-1–025502-4.
26. Koga K, Tanaka H (2005) Phase diagram of water between hydrophobic surfaces. *J Chem Phys* 122:104711.
27. Petrenko VF, Whitworth RW (1999) *Physics of Ice* (Oxford Univ Press, New York).
28. Halperin BI, Nelson DR (1978) Theory of two-dimensional melting. *Phys Rev Lett* 41:121–124.
29. Wang J, Yoo S, Bai J, Morris JR, Zeng XC (2005) Melting temperature of ice I_h calculated from coexisting solid-liquid phases. *J Chem Phys* 123:036101–1–2.
30. Giovambattista N, Rossky PJ, Debenedetti PG (2009) Phase transitions induced by nanoconfinement in liquid water. *Phys Rev Lett* 102:050603-1–050603-4.
31. Poole PH, Sciortino F, Essmann U, Stanley HE (1992) Phase behaviour of metastable water. *Nature* 360:324–328.
32. Tanaka H (1996) A self-consistent phase diagram for supercooled water. *Nature* 380:328–330.
33. Mishima O, Stanley HE (1998) The relationship between liquid, supercooled and glassy water. *Nature* 396:329–335.
34. Ito K, Moynihan CT, Angell CA (1999) Thermodynamic fragility in liquids and a fragile-to-strong liquid transition in water. *Nature* 398:492–495.
35. Smith RS, Kay BD (1999) The existence of supercooled water at 150 K. *Nature* 398:788–791.
36. Mishima O, Suzuki Y (2002) Propagation of the polyamorphic transition of ice and the liquid-liquid critical point. *Nature* 419:599–603.
37. Debenedetti PG, Stanley HE (2003) Supercooled and glassy water. *Phys Today* 56:40–46.
38. Ludwig R (2006) The puzzling properties of supercooled and glassy water. *Angew Chem Int Edit* 45:3402–3405.
39. Ball P (2008) Juggling with liquids. *Nat Mater* 7:928.
40. Ostwald WZ (1897) Studien über die Bildung und Umwandlung fester Körper. *Z Phys Chem* 22:289–330.
41. Cung S-Y, Kim Y-M, Kim J-G, Kim Y-J (2009) Multiphase transformation and Ostwald's rule of stages during crystallization of a metal phosphate. *Nat Phys* 5:68–73.
42. Mahoney MW, Jorgensen WL (2000) A five-site model for liquid water and the reproduction of the density anomaly by rigid, nonpolarizable potential functions. *J Chem Phys* 112:8910–8922.
43. Steele WA (1974) Interaction of gases with solid surface. (Pergamon, Oxford).
44. Kumar P, Buldyrev SV, Starr FW, Giovambattista N, Stanley HE (2005) Thermodynamics, structure, and dynamics of water confined between hydrophobic plates. *Phys Rev E* 72:051503-1–051503-12.
45. Hummer G, Rasaiah JC, Noworyta JP (2001) Water conduction through the hydrophobic channel of a carbon nanotube. *Nature* 414:188–191.
46. Walsh MR, Koh CA, Sloan ED, Sum AK, Wu DT (2009) Microsecond simulations of spontaneous methane hydrate nucleation and growth. *Science* 326:1095–1098.

Supporting Information

Bai et al. 10.1073/pnas.0906437107

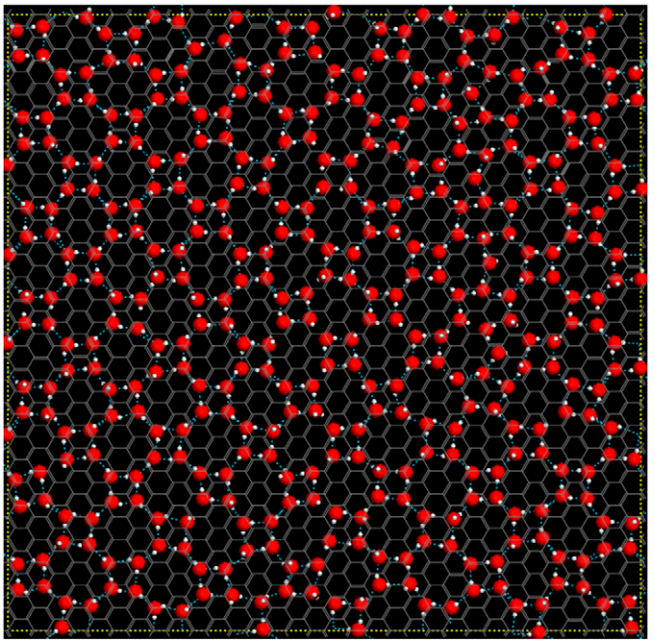

Fig. S1. A snapshot (at 8 ns) of 2D monolayer low-density ice (LDI) formed in between two single graphene layers (gray hexagon network). Red spheres represent oxygen atoms and white spheres represent hydrogen atoms. The distance between the two graphene layers is $D = 0.65$ nm. The geometric pattern of the LDI is identical to *Archimedean* $4 \cdot 8^2$ truncated square tiling, composed of water tetragons and octagons. The temperature of the system is fixed at 210 K.

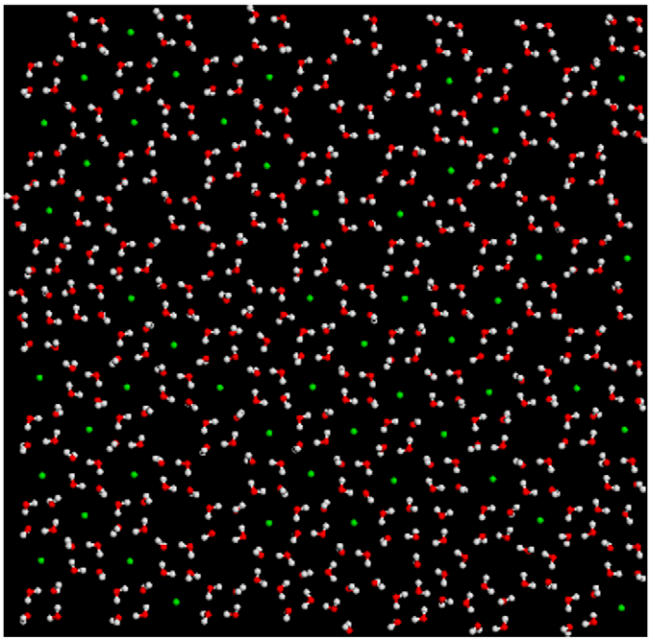

Movie S1. A video of molecular dynamics (MD) computer experiment of the formation of monolayer ice clathrate in a slit nanopore. The green particles are argon atoms.

Movie S1 (MPG)

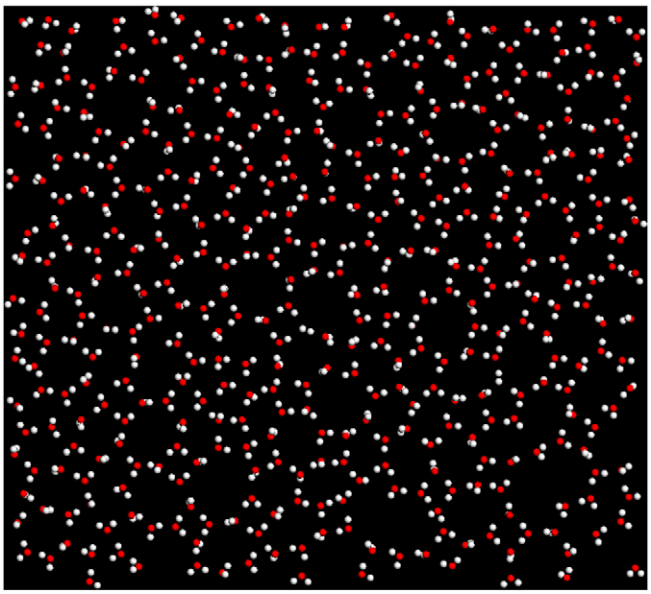

Movie S2. A video of MD computer experiment of the formation of monolayer low-density ice in a slit nanopore.
Movie S2 (MPG)

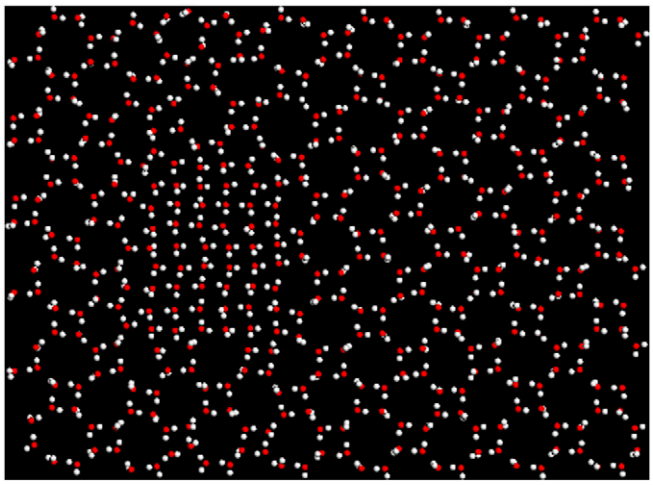

Movie S3. A video of MD computer experiment of a low-density ice (containing a high-density ice grain) under a compression. Eventually it transforms into a high-density ice.
Movie S3 (MPG)

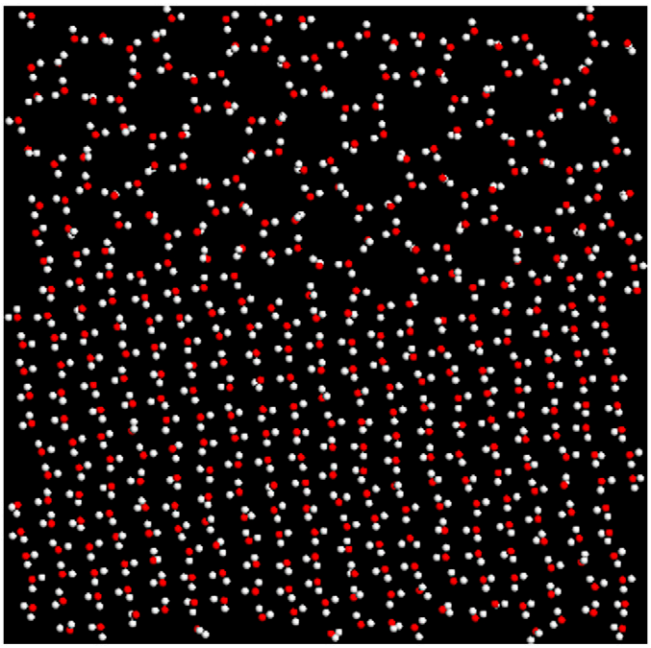

Movie S4. A video of MD computer experiment of a coexisting high-density/low-density ice under a strong tension. Eventually it transforms into a low-density ice.

Movie S4 (MPG)

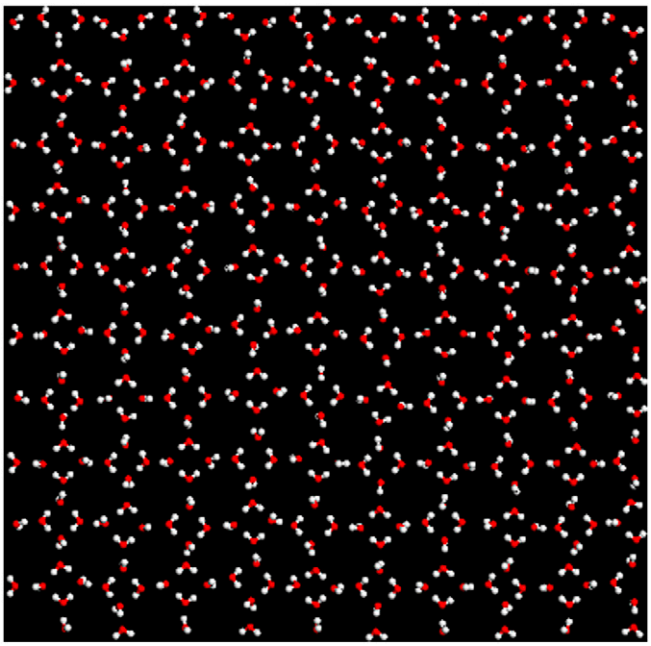

Movie S5. A video of MD computer experiment of a low-density ice under a strong compression. Eventually it transforms into a high-density ice.

Movie S5 (MPG)